Metal-to-Ligand Electron Transfer in Diiminopyridine Complexes of Mn−Zn. A Theoretical Study

Peter H. M. Budzelaar,*,† Bas de Bruin, and Anton W. Gal

Department of Inorganic Chemistry, University of Nijmegen, Toernooiveld 1, 6525 ED Nijmegen, The Netherlands

Karl Wieghardt

Max-Planck-Institut für Strahlenchemie, Stiftstrasse 34−36, D-45470 Mülheim an der Ruhr, Germany

Joop H. van Lenthe‡

Theoretical Chemistry Group, University of Utrecht, Padualaan 14, 3584 CH Utrecht, The Netherlands

Received December 27, 2000

A series of complexes ML_2^{x+} (M = Mn−Zn, L = 2,6-bis(iminomethyl)pyridine) was investigated by theoretical methods. Electron transfer from the metal "t_{2g}" orbitals to the ligand π^* orbitals is reflected in the elongation of ligand C−N bonds and shortening of the C_{py}−C_{imine} bonds. Using zinc complexes as references, these deformations could be used to quantify the number of electrons transferred. Strong transfer is found in low-spin MnL_2^+ (ca. 2 *e*) and in high-spin MnL_2^+ and low-spin MnL_2^{2+}, FeL_2^{2+}, and CoL_2^+ (ca. 1 *e* each). Smaller transfer is found in CoL_2^{2+}, and the transfer is insignificant in high-spin MnL_2^{2+}, NiL_2^{2+}, and CuL_2^{2+}. Analysis of the unpaired electron density on the metal (using the Staroverov−Davidson method) shows that the contribution of a biradical description, in which ligand radical anions are antiferromagnetically coupled to the metal center, is significant in most cases. In the case of CoL_2^+ and high-spin MnL_2^+, where the metal−ligand bond is weakened, it amounts to over 50% of the total transfer.

Introduction

Redox reactions of transition metal complexes can be complicated by the fact that both metal- and ligand-centered oxidation and reduction are possible. In fact, subtle alternation between ligand- and metal-centered reactions plays a crucial role in many biological redox processes. The question of which of the two alternatives applies is not always easy to answer, even for well-defined model systems.

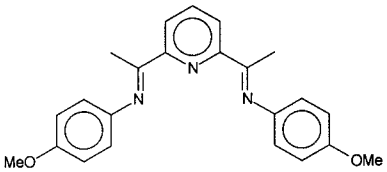

L_{Ar}

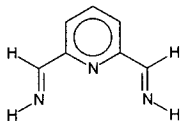

L_H

We recently reported on the redox chemistry of first-row transition metal complexes (Mn−Zn) of the 2,6-diiminopyridine ligand L_{Ar}.[1] The observed complexes of the type $M(L_{Ar})_2^{2+}$ apparently always contained a divalent metal ion and neutral ligands, but evidence for ligand-centered reduction was found for several reduced species. The redox chemistry of $Mn(L_{Ar})_2^{2+}$ (**A**) was of particular interest, since it seemed to follow the ECEC type pathway shown in Scheme 1.

The X-ray structure of the reduced complex $Mn(L_{Ar})_2^+$ agreed with the interpretation as $Mn^{III}(L^-)_2$ (**C**). However, structural parameters could not be used to distinguish between two alternative descriptions of the electronic structure: (1) Electrons paired, a delocalized model in which all electrons are paired but delocalized over Mn "t_{2g}" and ligand π^* orbitals (*back-donation* model). (2) Electrons unpaired, a low-spin Mn^{III} ion (S = 1) antiferromagnetically coupled to two ligand radical anions L^-, yielding a singlet ground state (*biradical* model).

It should be noted here that the distinction between these alternatives is not absolute: *every* bond has some degree of biradical character, and the above descriptions are just the extremes of a continuum of possibilities. The two extremes are easily described in MO terms as closed-shell and open-shell singlet configurations, respectively. Intermediate situations, however, cannot be described by a single configuration and are best represented schematically as a *mixture* of two configurations (see Scheme 2).[2,3]

In such a situation, the two electrons are *partially* unpaired but still give rise to a singlet state. In the present case, an added

† E-mail: budz@sci.kun.nl.
‡ E-mail: joop@chem.uu.nl.

(1) De Bruin, B.; Bill, E.; Bothe, E.; Weyhermuller, T.; Wieghardt, K. *Inorg. Chem.* **2000**, *39*, 2936.

(2) In Scheme 2, $c_1 = 1$, $c_2 = 0$ corresponds to the pure back-donation model, $c_1 = c_2 = \sqrt{2}$ to the pure biradical situation. In a valence-bond picture, the intermediate situation has one electron partly localized in a metal 3d orbital (but still with some ligand π^* character), coupled to one electron partly localized in the ligand π^* orbital (but with still some metal 3d character).

10.1021/ic001457c CCC: $20.00
Published on Web 07/31/2001

Scheme 1. Redox Cycle Proposed for MnL_2^{2+} [1]

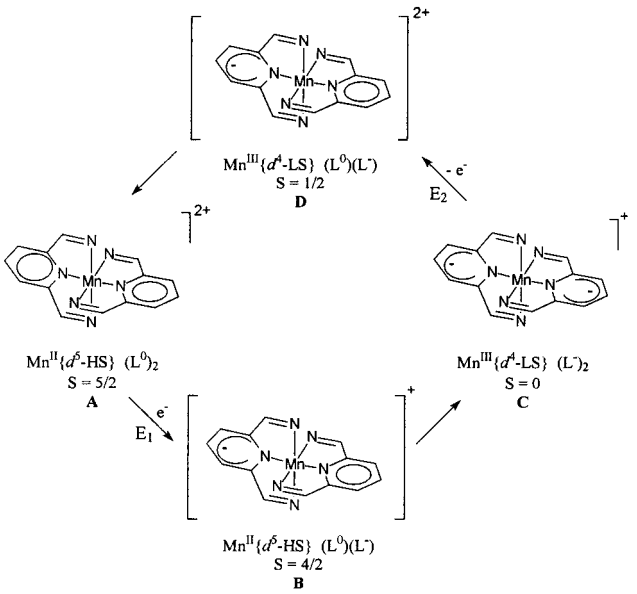

Scheme 2. Schematic Representations of (A) Backdonation, (B) Biradical, and (C) Intermediate Situations. In (A), the Arrows Indicate the 3d → π^* Back-Donation

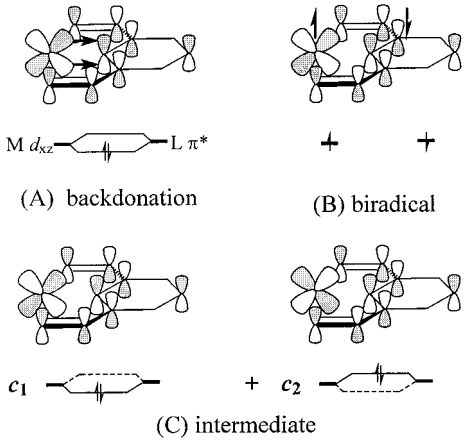

complication is that we have to consider electron transfer from *all three* metal "t_{2g}" orbitals (Scheme 3), each of which can be accompanied by partial unpairing.

Here we report a theoretical study of complexes of the model ligand L_H with the metals Mn to Zn. This study has the following goals: (1) To check what level of theory is required to reproduce the structural data reported for the $M(L_{Ar})_2$ complexes. (2) To check the earlier interpretation[1] of the redox behavior of the Mn complex. (3) To quantify the amount of metal-to-ligand electron transfer in different complexes. (4) To distinguish between back-donation and biradical descriptions of the reduced Mn complex MnL_2^+, and to compare this species with the isoelectronic FeL_2^{2+} complex.

Calculations

General. All calculations were carried out with the GAMESS-UK program[4] on SGI workstations. The minimal sto-3g basis[5] and the small split-valence 3-21G basis[6] were used for the first-row atoms. For the metals Mn to Zn and for Br, we used relativistic effective core potentials (for the inner core orbitals) and the LANL2DZ basis (for the valence and outer core electrons).[7] Geometries were optimized without symmetry constraints at the restricted or unrestricted B3LYP[8]/sto-3g level; within the symmetries resulting from these calculations, the structures were then re-optimized at the B3LYP/3-21g level. Total energies from all B3LYP calculations are listed in the Supporting Information (Table S7); geometrical parameters for all optimized structures are available from one of the authors (P.H.M.B.) on request. Key geometrical parameters for the 3-21G optimizations are given in Tables 1 and 2; the corresponding sto-3g data are given in the Supporting Information (Tables S4 and S5). For D_{2d}-symmetric complexes ML_2^{x+}, the unique *z*-axis is along $N_{Py}-M-N_{Py}$ and the two ligands lie in the *xz* and *yz* planes.

Unpaired Electron Density Analysis. We decided to create ab initio correlated wave functions based on the B3LYP orbitals for use in the unpaired electron density (UED) analysis developed by Staroverov and Davidson.[9] For the closed-shell systems, the procedure is straightforward. The B3LYP orbitals can be used as they are in the ab initio calculations. A first (single-reference) SDCI (using ca. 45 highest occupied and ca. 50 lowest unoccupied orbitals) produced a set of important configurations (coefficient > 0.03). These were included in the reference set for the next multireference CI, and the procedure was repeated until no new important configurations were found (usually 2 or 3 iterations were sufficient). The natural orbitals from the final MR-SDCI (involving usually $1-3 \times 10^7$ configurations) were then used for the UED analysis.

For the open-shell systems, the situation is less straightforward. The unrestricted B3LYP calculation produces separate sets of α and β orbitals, which cannot be used directly in a CI calculation. The spin-free natural orbitals from the UB3LYP calculation[10] form a well-defined set, but since they are characterized by occupation number instead of by energy it is difficult to make a selection of CI active orbitals within nearly degenerate sets. Therefore, we first divided them into sets having nearly equal occupation numbers. Within each set, the orbitals were then canonicalized using the B3LYP Fock operator.[11,12] In most cases, spin contamination in the UB3LYP calculations is small and there were just three sets with occupation number ranges 2.00−1.98, 0.99−1.01, and 0.02−0.00. The canonicalization provides an energy ordering of the orbitals analogous to the "standard" ordering of RB3LYP orbitals for the closed-shell case. A set of the highest occupied and lowest

(3) For a more quantitatively accurate description at the ab initio level, many more configurations are needed. In fact, limited GVB or MCSCF treatments of these systems do not reproduce the mixture of ligand and metal orbitals at all. This is why the simple two-configuration picture shown could not be used directly as the basis for a calculation.

(4) GAMESS-UK is a package of ab initio programs written by Guest, M. F.; Van Lenthe, J. H.; Kendrick, J.; Schoffel, K.; Sherwood, P. with contributions from Amos, R. D.; Buenker, R. J.; Van Dam, H. J. J.; Dupuis, M.; Handy, N. C.; Hillier, I. H.; Knowles, P. J.; Bonacic-Koutecky, V.; Von Niessen, W.; Harrison, R. J.; Rendell, A. P.; Saunders, V. R.; Stone, A. J.; De Vries, A. H. The package is derived from the original GAMESS code due to Dupuis, M.; Spangler, D.; Wendoloski, J.: NRCC Software Catalog, Vol. 1, Program No. QG01 (GAMESS), 1980. Direct-CI: Saunders: V. R.; Van Lenthe, J. H. *Mol. Phys.* **1983**, *48*, 923; the DFT module was developed by , P. Young under the auspices of EPSRC's Collaborative Computational Project No. 1 (CCP1) (1995−1997).
(5) Hehre, W. J.; Stewart, R. F.; Pople, J. A. *J. Chem. Phys.* **1969**, *51*, 2657.
(6) Binkley, S.; Pople, J. A.; Hehre, W. J. *J. Am. Chem. Soc.* **1980**, *102*, 939.
(7) Hay, P. J.; Wadt, W. R. *J. Chem. Phys.* **1985**, *82*, 299.
(8) Becke, A. D. *J. Chem. Phys.* **1993**, *98*, 5648.
(9) Staroverov, V. N.; Davidson, E. R. *J. Am. Chem. Soc.* **2000**, *122*, 186. Staroverov, V. N.; Davidson, E. R. *Int. J. Quantum Chem.* **2000**, *77*, 316. Staroverov, V. N.; Davidson, E. R. *Int. J. Quantum Chem.* **2000**, *77*, 651. Staroverov, V. N.; Davidson, E. R. *J. Am. Chem. Soc.* **2000**, *122*, 7377.
(10) A spin-free density matrix is obtained by integrating over the spin of the UB3LYP "density matrix", and diagonalization gives spin-free natural orbitals. Natural orbitals derived in this way from UHF orbitals have been shown to be a very suitable basis for CASSCF calculations: Pulay, P.; Hamilton, T. P. *J. Chem. Phys.* **1988**, *88*, 4926. Bofill, J. M.; Pulay, P. *J. Chem. Phys.* **1989**, *90*, 3637.
(11) Canonicalization is the transformation of a set of orbitals to eigenfunctions of a 1-electron operator.
(12) The canonicalization procedure will be described separately in a future paper.

Scheme 3. Back-Donation (Indicated by Arrows) from the Three Metal "t_{2g}" Orbitals to Ligand π^* Orbitals

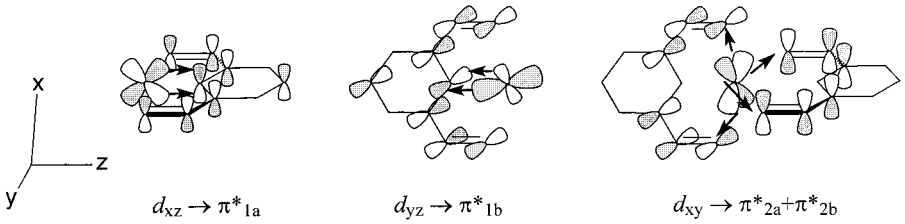

Table 1. *Observed* (L_{Ar}; X-ray)[a] and Calculated (L_H; B3LYP/3-21G)[b] Bond Lengths (Å)

				pyridine				imine		
metal	charge	spin	symmetry	$N_{py}-M$	$N_{py}-C_\alpha$	$C_\alpha-C_\beta$	$C_\beta-C_\gamma$	$N_{im}-M$	$N_{im}-C_{im}$	$C_{im}-C_\alpha$
Mn	**+2**	5/2	$\approx D_{2d}$	*2.174*	*1.338*	*1.392*	*1.383*	*2.263*	*1.283*	*1.498*
		5/2	D_{2d}	2.205	1.346	1.397	1.400	2.301	1.288	1.479
		1/2	C_2[c]	1.924	1.362	1.393	1.405	2.047	1.300	1.461
					1.360	1.401	1.398	2.009	1.305	1.453
Mn	**+1**	0	$\approx D_{2d}$	*1.885*	*1.373*	*1.392*	*1.392*	*1.984*	*1.321*	*1.442*
		0	D_{2d}	1.902	1.377	1.396	1.399	1.978	1.311	1.442
		4/2	D_{2d}	2.159	1.361	1.396	1.401	2.290	1.300	1.457
Fe	**+2**	0	$\approx D_{2d}$	1.868	1.353	1.389	1.390	1.987	1.309	1.467
		0	D_{2d}	1.907	1.355	1.397	1.402	1.998	1.298	1.467
Co	**+2**	1/2	$\approx C_{2v}$[d]	*1.852*	*1.349*	*1.390*	*1.387*	*2.015*	*1.302*	*1.474*
				1.911	*1.349*	*1.387*	*1.388*	*2.155*	*1.289*	*1.486*
		1/2	C_{2v}[d]	1.892	1.353	1.396	1.402	2.013	1.295	1.469
				1.953	1.354	1.397	1.399	2.235	1.286	1.474
Co	**+1**	2/2	$\approx D_{2d}$	*1.990*	*1.357*	*1.390*	*1.382*	*2.145*	*1.303*	*1.465*
		2/2	D_{2d}	2.034	1.359	1.395	1.399	2.185	1.294	1.460
Ni	**+2**	2/2	$\approx D_{2d}$	*1.969*	*1.341*	*1.388*	*1.386*	*2.218*	*1.290*	*1.492*
		2/2	D_{2d}	2.025	1.345	1.397	1.401	2.163	1.288	1.479
Cu	**+2**	1/2	$\approx C_{2v}$[d]	*1.942*	*1.340*	*1.387*	*1.387*	*2.161*	*1.291*	*1.494*
				1.956	*1.342*	*1.388*	*1.385*	*2.223*	*1.290*	*1.491*
		1/2	C_{2v}[d]	1.987	1.348	1.397	1.400	2.182	1.286	1.476
				2.015	1.351	1.397	1.398	2.310	1.283	1.477
Zn	**+2**	0	$\approx D_{2d}$	*2.042*	*1.336*	*1.391*	*1.388*	*2.199*	*1.285*	*1.502*
		0	D_{2d}	2.142	1.343	1.398	1.400	2.268	1.286	1.482
Zn	**+1**	1/2	D_2[e]	2.109	1.358	1.395	1.402	2.271	1.299	1.460
	(0)	2/2or 0[f]	D_{2d}[g]	2.091	1.375	1.392	1.405	2.291	1.312	1.442
(free L)	**(0)**	0	$\approx C_{2v}$		*1.343*	*1.403*	*1.374*		*1.274*	*1.501*
		0	C_{2v}		1.348	1.403	1.393		1.278	1.483
	−1	1/2	C_{2v}		1.393	1.398	1.404		1.307	1.455
			C_{2v}[h]		1.351	1.452	1.391		1.309	1.451
$BrMn(CO)_2L$		0	$\approx C_s$	*1.944*	*1.354*	*1.398*	*1.387*	*1.996*	*1.288*	*1.467*
		0	C_s	1.921	1.361	1.396	1.399	1.980	1.306	1.452

[a] X-ray data from refs 1 ($M(L_{Ar})_2$ complexes), 20 (free L_{Ar}), and 16 ($BrMn(CO)_2L_{Ph}$). [b] B3LYP; 3-21G basis on CHON, LANL2DZ small core on metal. [c] Two sides of each ligand inequivalent. [d] Ligands inequivalent due to Jahn−Teller distortion. [e] Ligand ($\pi^*_{1a} + \pi^*_{1b}$) occupied. [f] "Singlet" and triplet optimize to same geometry. [g] Ligand π^*_{1a},π^*_{1b} occupied. [h] Ligand LUMO+1 (π^*_2) occupied.

unoccupied orbitals obtained in this way was then used for the MR-SDCI calculation and UED analysis, just as in the closed-shell case.

Results and Discussion

Geometries of Complexes. The most critical species in this study are high-spin MnL_2^{2+} (**A**) and low-spin MnL_2^+ (**C**), since they illustrate how delicate the balance between population of metal 3d and ligand π^* orbitals is. Therefore, we started with these two species. The geometry of MnL_2^{2+} was already reproduced reasonably well at the ROHF level. However, RHF calculations on low-spin MnL_2^+ did not reproduce the ligand deformation observed in the X-ray structure, nor did they show enough shortening of the Mn−N bonds, indicating that at this level the Mn 3d levels are too far below the ligand π^* levels. If the interpretation given earlier is correct, a better description would use two GVB pairs for the Mn 3d−ligand π^* combinations, but at ROHF-GVB the energy levels of these orbitals were found to be too far apart to mix and the GVB description did not yield any improvement.

UHF reproduced the structure of MnL_2^+ reasonably well, including ligand deformation and short Mn−N bonds. However, this was accompanied by strong spin contamination. In addition, UHF predicted a similar deformation for MnL_2^{2+}, where it is not observed experimentally. Clearly, neither RHF nor UHF gets the balance between metal and ligand levels right. Going to correlated levels (e.g., MP2) would then be problematic, since these are still based on (qualitatively incorrect) Hartree−Fock orbitals.

Therefore, we resorted to DFT (B3LYP) for these systems. The experimental geometries could be reproduced nicely, and at the same time the orbitals showed a strong donation from metal 3d to ligand π^* for MnL_2^+ but not for MnL_2^{2+}, as detailed below. Thus, the balance between metal and ligand levels is now such that it can reproduce the observed deformations. Calculated and observed geometries are compared in Tables 1 and S4. At the minimal-basis B3LYP/sto-3g level (Table S4), the C−N distances are systematically too long by ca. 0.05 Å; at the split-valence B3LYP/3-21G level (Table 1), metal−nitrogen distances are systematically too long (typically by 0.02−0.04 Å). Apart from that the agreement is remarkable. Even the Jahn−Teller distortions of CoL_2^{2+} and CuL_2^{2+} are reproduced correctly.[13] In the remainder of the text we will only

Table 2. *Observed* (L_{Ar}; X-ray) and Calculated (L_H; B3LYP/3-21G) Bond Length Deformations (in Å; Relative to ZnL_2^{2+}) and Fitted Electron Transfer[a]

			pyridine			imine		transfer
metal	charge	spin	$N_{py}-C_\alpha$	$C_\alpha-C_\beta$	$C_\beta-C_\gamma$	$N_{im}-C_{im}$	$C_{im}-C_\alpha$	no. of *e*
Mn	**+2**	5/2	*+0.002*	*+0.001*	*−0.005*	*−0.002*	*−0.004*	*0.07(8)*
		5/2	+0.003	−0.001	0	+0.002	−0.003	0.16(2)
		1/2	+0.019	−0.005	+0.005	+0.014	−0.021	
			+0.017	+0.003	−0.002	+0.019	−0.029	1.17(9)
Mn	**+1**	0	*+0.037*	*+0.001*	*+0.004*	*+0.036*	*−0.060*	*(2)*
		0	+0.034	−0.002	−0.001	+0.025	−0.040	1.93(14)
		4/2	+0.018	−0.002	+0.001	+0.014	−0.025	1.13(4)
Fe	**+2**	0	*+0.017*	*−0.002*	*+0.002*	*+0.024*	*−0.035*	*1.14(8)*
		0	+0.012	−0.001	+0.002	+0.012	−0.015	0.76(5)
Co	**+2**	1/2	*+0.013*	*−0.001*	*−0.001*	*+0.017*	*−0.028*	
			+0.013	*−0.004*	*0*	*+0.004*	*−0.016*	*0.69(6)*
		1/2	+0.010	−0.002	+0.002	+0.009	−0.013	
			+0.011	−0.001	−0.001	0	−0.008	0.51(6)
Co	**+1**	2/2	*+0.021*	*−0.001*	*−0.006*	*+0.018*	*−0.037*	*1.15(12)*
		2/2	+0.016	−0.003	−0.001	+0.008	−0.022	0.94(9)
Ni	**+2**	2/2	*+0.005*	*−0.003*	*−0.002*	*+0.005*	*−0.010*	*0.30(5)*
		2/2	−0.002	+0.001	+0.001	+0.002	−0.003	0.07(6)
Cu	**+2**	1/2	*+0.004*	*−0.004*	*−0.001*	*+0.006*	*−0.008*	
			+0.006	*−0.003*	*−0.003*	*+0.005*	*−0.009*	*0.28(4)*
		1/2	+0.002	−0.001	−0.002	−0.003	−0.005	
			+0.005	−0.001	0	0	−0.006	0.17(5)
Zn	**+2**	0	-	-	-	-	-	(0)
		0	-	-	-	-	-	(0)
Zn	**+1**	1/2 (D_2)	+0.015	−0.003	+0.002	+0.013	−0.022	(1)
Zn	**(0)**	2/2 or 0	+0.032	−0.006	+0.005	+0.026	−0.040	1.94(7)
$BrMn(CO)_2L$		0	*+0.018*	*+0.007*	*−0.001*	*+0.003*	*−0.035*	*0.46(11)*
		0	+0.018	−0.002	−0.001	+0.020	−0.030	0.67(5)

[a] For remarks on individual structures, see Table 1.

refer to the 3-21G results; the corresponding sto-3g results are listed in the Supporting Information.

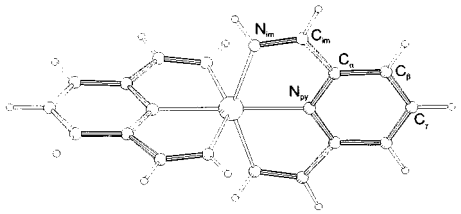

For most complexes we calculate completely symmetric (D_{2d}) structures; the exceptions are as follows: (1) Low-spin MnL_2^{2+} shows a slight distortion to C_2 symmetry. We cannot explain this distortion at present; there is no obvious orbital explanation for it. The orbital occupations are not consistent with a Jahn−Teller distortion. (2) CoL_2^{2+} and CuL_2^{2+} show a Jahn−Teller distortion resulting in C_{2v}-symmetric structures with inequivalent diiminopyridine ligands, one of which has significantly longer $M-N_{imine}$ distances. The additional electron in the "e_g" set (compared to ML_2^{3+}) occupies a d_{z^2}-like orbital which is antibonding between the metal and these imines.

None of the experimental structures[1] has crystallographically imposed symmetry elements. However, the deviations from ideal D_{2d} or C_{2v} symmetry are small and can be ascribed to packing effects.

Redox Behavior of MnL_2^{2+}. Our calculations on $Mn(L_H)_2^{2+}$ and $Mn(L_H)_2^{+}$ support the assignment of the species shown in Scheme 1. At the B3LYP level, the high-spin state of MnL_2^{+} (**B**, S = $^4/_2$) is higher in energy than the low-spin state (**C**), whereas for MnL_2^{2+} the reverse is true (**D**, S = $^1/_2$ above **A**, S = $^5/_2$). Analysis of the geometries (see below) shows that metastable species **B** and **D** have approximately one electron on the two ligands together, whereas **C** has two and **A** has none. Thus, both reduction of high-spin MnL_2^{2+} and oxidation of low-spin MnL_2^{+} are initially ligand-centered. The changes in M−N distances associated with these redox reactions are modest. The subsequent changes in spin state, however, are accompanied by dramatic changes in the M−N bond lengths (>0.2 Å!). This may contribute to the presence of significant barriers for the spin flips.

The balanced free energy equation for the redox cycle in Scheme 1 can be written as

$$\Delta G_1(\mathbf{A}\rightarrow\mathbf{B}) - \Delta G_3(\mathbf{D}\rightarrow\mathbf{C}) = -F(E_1 - E_2) = \Delta G_2(\mathbf{C}\rightarrow\mathbf{B}) + \Delta G_4(\mathbf{A}\rightarrow\mathbf{D})$$

Thus, from the reported estimated range of redox potentials for the couples **A**/**B** (E_1 between −1.31 and −1.55 V) and **D**/**C** (E_2 between −0.52 and −0.28 V) one can estimate the sum of the free energies $\Delta G_2(\mathbf{C}\rightarrow\mathbf{B}) + \Delta G_4(\mathbf{A}\rightarrow\mathbf{D})$ to be in the range +18.2 to +29.3 kcal/mol. The agreement with our B3LYP value of +18.8 kcal/mol[14] is surprisingly good and must in part be fortuitous. Nevertheless, this provides additional support for the surprising conclusion[1] that *reduction* of a single ligand of MnL_2^{2+} induces spontaneous *oxidation* of the metal.

Orbital Interactions in ML_2^{x+} Complexes. The diiminopyridine ligand is not only a good σ-donor but also a π-acceptor. The low-lying π-acceptor orbitals (π^*_1, π^*_2) of the free ligand L_H are shown in Figure 1. They are rather close in energy, and the calculations predict the radical-anions derived from population of LUMO (π^*_1) and LUMO+1 (π^*_2) to have nearly the same energy.

(13) At the B3LYP/sto-3g level, the optimized structure of CuL_2^{2+} has D_{2d} symmetry, because the Jahn−Teller unique axis is along the Py-Cu−Py vector. However, at the B3LYP/3-21G level the elongation along *one* imine-Cu−imine axis is reproduced correctly.

(14) Calculated from the total energies in Table S7; no zero-point energies and thermal corrections included.

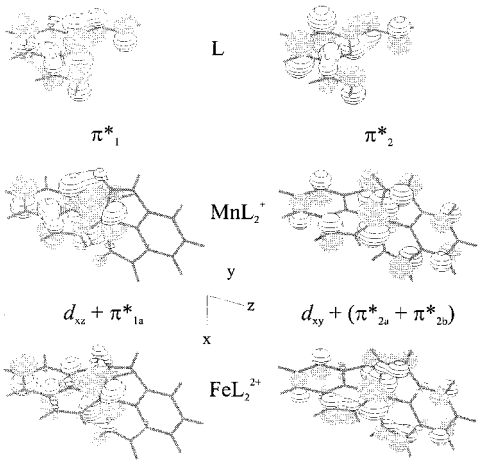

Figure 1. π-Acceptor orbitals of the ligand L; "t_{2g}" orbitals of MnL_2^+ and FeL_2^{2+} (the *z*-axis is along $N_{Py}-M-N_{Py}$; the ligands lie in the *xz* and *yz* plane).

In the series of L_2M complexes, each orbital of the metal "t_{2g}" set can delocalize into exactly one ligand orbital (combination), as shown in Figure 1 for MnL_2^+ and FeL_2^{2+}:

$$d_{xz} \text{ into } \pi^*_{1a}$$

$$d_{yz} \text{ into } \pi^*_{1b}$$

$$d_{xy} \text{ into } (\pi^*_{2a} + \pi^*_{2b})$$

Here the a and b subscripts denote the two ligands. Since the d_{xz} and d_{yz} orbitals are symmetry-related, we show only one of the two in Figure 1.[15] The orbital drawings show that delocalization is substantial in MnL_2^+ and in FeL_2^{2+}; it decreases on moving in the direction of Zn. Delocalization from d_{xy} is always smaller than from the d_{xz},d_{yz} pair.

Magnitude of Metal-to-Ligand Electron Transfer. Regardless of the nature of the metal−ligand interaction (biradical or back-donation), population of the ligand π^* orbitals will result in geometric deformations. Deformations relative to L_H in $Zn(L_H)_2^{2+}$, where transfer is assumed to be negligible, have been collected in Table 2. If we assume that in the reduced complex $Zn(L_H)_2^+$ the additional electron is located entirely on the ligands, we can use the structure of this species as a calibration point for relating deformations to metal-to-ligand electron transfer. Least-squares fits of the deformations calculated for the other complexes (using all relevant C−C and C−N bond lengths) give the magnitudes of transfer from the metal 3d to ligand π^* orbitals. Typical standard deviations in these fits are 0.04−0.1 *e*, with errors of about 0.003 Å in the fitted bond lengths. The quality of the fits shows that deformations in the transition metal complexes can indeed be attributed to partial population of ligand π^* orbitals. The results (also in Table 2) show that transfer is negligible in high-spin MnL_2^{2+} but amounts to nearly two electrons in low-spin MnL_2^+. Interestingly, the metastable high-spin MnL_2^+ and low-spin MnL_2^{2+} both show a transfer of ca. 1 electron. This is all perfectly in line with the ECEC cycle of Scheme 1. Electron transfer is small in NiL_2^{2+} and CuL_2^{2+} but becomes larger in CoL_2^{2+}; in FeL_2^{2+} and CoL_2^+ it comes close to a full electron. Electron-transfer magnitudes calculated from Mulliken populations of the metal 3d orbitals (see Table S6) show a similar trend, although the numerical values are different. However, in the present work we will only refer to the values derived from the geometric analysis, since they do not depend on any arbitrary basis set partitioning and are more easily compared to experiment.

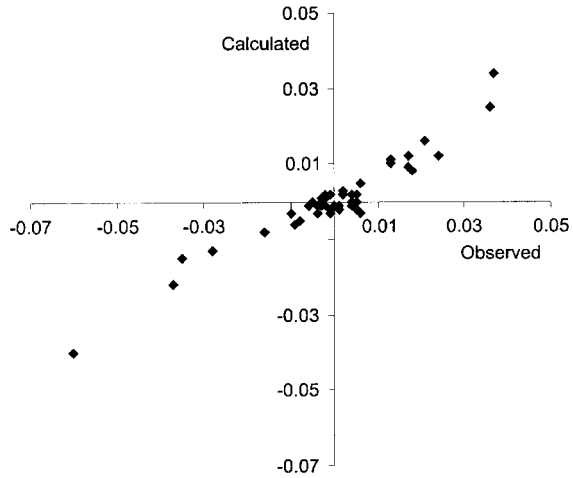

Figure 2. Calculated (B3LYP/3-21G) vs observed (X-ray) bond deformations (Å) in ML_2 complexes.

For the experimental results, we can use $Zn(L_{Ar})_2^{2+}$ as a reference, but there is no unambiguous calibration point for a singly or doubly reduced ligand, since the reduced Zn complexes were too unstable to allow isolation.[1] One might consider using the calculated deformation for $Zn(L_H)_2^+$ as a reference, but this turns out to be unsatisfactory. The *trends* in the deformations are similar for the calculated and experimental structures, but the *magnitudes* of the deformations in the calculated structures are about 30% smaller than in the corresponding experimental structures (see Figure 2). This might be due to the limited basis set employed, since deformations calculated at the sto-3g level tend to be even smaller (Table S5). It might also be caused by the use of the model ligand L_H for L_{Ar}. Therefore, we decided to calibrate the experimental results to a transfer of 2.0 *e* for $Mn(L_{Ar})_2^+$, close to the value obtained for $Mn(L_H)_2^+$ from the theoretical fits. Because the random "errors" in the experimental X-ray data (combined packing effects and refinement errors) are larger than the random errors in the calculations, the errors in the fitted bond lengths are also somewhat larger (typically 0.006 Å). In view of this, the agreement between the transfers obtained from calculated and experimental structures is reasonable. These results support the assumption that electron transfer is the main determinant of the bond length changes.

For comparison, we have also calculated the structure of $BrMn(CO)_2L_H$ as a model for $BrMn(CO)_2L_{Ph}$, the only other formal Mn^I complex of a diiminopyridine ligand for which a structure has been reported to date.[16] That X-ray structure has relatively large errors bars, but it shows roughly the same type of ligand deformation as the ML_2 complexes that are the focus of this paper. The amount of electron transfer to the diiminopyridine ligand is $^1/_2$ *e*, i.e., significantly lower than that to each ligand of low-spin MnL_2^+. Mulliken population analyses (Table S6) indicate that back-donation to the carbonyl ligands is also important here.

The *magnitude* of the transfer depends primarily on two factors. (1) The relative energies of metal 3d and ligand π^* orbitals: lower 3d energies will result in less transfer. This is illustrated by the series of $(t_{2g})^6(e_g)^n$ L_2M^{2+} complexes (M =

(15) The orbitals shown in the figure are not symmetry-adapted. The localized versions illustrate more clearly the donation from a single metal d-orbital to a ligand π^* orbital. The equivalent symmetry-adapted version would show the back-donation from $(d_{xz} + d_{yz})$ to $(\pi^*_{1a} + \pi^*_{1b})$ and from $(d_{xz} - d_{yz})$ to $(\pi^*_{1a} - \pi^*_{1b})$.

(16) Stor, G. J.; Van de Vis, M.; Stufkens, D. J.; Oskam, A.; Fraanje, J.; Goubitz, K. *J. Organomet. Chem.* **1994**, *482*, 15.

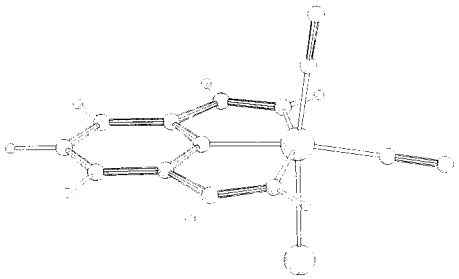

Fe,Co,Ni). with decreasing transfer. (2) The spin pairing patterns of the metal 3d orbitals: electrons paired in metal 3d "t_{2g}" orbitals will have a higher tendency to delocalize to the ligand in order to avoid intra-pair repulsion. This is illustrated by the strong transfer found in the low-spin states of L_2Mn^{2+} and L_2-Mn^{+}.

Calculation of Biradical Character. The distinction between biradical and back-donation models is a rather subtle one. In favorable cases, the interpretation of the electronic structure can be obvious. A nice example of such a clear-cut case is the semiquinone complex studied by Rodriguez et al.[17] There, triplet $(N_4)Cr(SQ)^{2+}$ (N_4 = tris(dimethylaminoethyl)amine) consists of a semiquinone radical antiferromagnetically coupled to a quartet Cr^{3+} center; the corresponding α and β orbitals were found to be strongly localized on ligand and metal, respectively. In the present case, the situation is less clear. As mentioned above, the geometry of MnL_2^{+} is reproduced satisfactorily at the restricted B3LYP level. At first sight, this would seem to indicate that the molecule is best described as a closed-shell system with extensive delocalization (back-donation) from Mn 3d orbitals to the ligand π* system, and *not* as the alternative biradical $Mn^{III}(d^4\text{-LS})(L^{-})_2$. However, B3LYP can prefer delocalized "closed-shell" descriptions even for systems having substantial biradical character,[9] so this conclusion may be premature.

Staroverov and Davidson recently proposed a method for calculating the "density of effectively unpaired electrons" and used this as a measure of biradical character.[9] We decided to apply their unpaired electron density (UED) analysis to our systems. Unfortunately, this calculation requires use of the full 1-*e* density *matrix* $\rho(\mathbf{x}'|\mathbf{x})$. DFT attempts to reproduce the density $\rho(\mathbf{x})$ (i.e., the *diagonal* of $\rho(\mathbf{x}'|\mathbf{x})$) without calculating the full density matrix; hence, it cannot be used for the Staroverov−Davidson analysis. Therefore, we wanted to use a correlated ab initio wave function for this analysis. One complication is that here the Hartree−Fock orbitals are qualitatively incorrect, casting doubt on the validity of low-level correlated wave functions derived from them. To overcome this problem, we performed multireference CI calculations based on the B3LYP orbitals. For the open-shell systems, where only unrestricted B3LYP orbitals were available, these were first transformed into canonicalized sets using the B3LYP Fock operator (see Calculations section). For both closed-shell and open-shell systems, the natural orbitals from the final MR-SDCI calculation were then analyzed with the method proposed by Staroverov and Davidson.

Biradical and Back-Donation Descriptions of ML_2^{x+} Complexes. The results of the analysis (Table 3) indicate that the UED on Mn in low-spin MnL_2^{+} is significant (0.72 *e*), though less than the value of ca. 2 expected for a true Mn^{III}-$(d^4\text{-LS})(L^{-})_2$ biradical description. For FeL_2^{2+}, we find a much smaller metal UED of only 0.23 *e*, closer to that in the reference

(17) Rodriguez, J. H.; Wheeler, D. E.; McCusker, J. K. *J. Am. Chem. Soc.* **1998**, *120*, 12051.

Table 3. Metal Unpaired Electron Density Analysis[a]

metal	charge	spin	reference conf[b]	UED	birad transfer	transfer from fit[c]	% birad transfer[d]
Mn	+2	5/2	$(t_{2g})^3(e_g)^2$	4.85	-	0.16	-
		1/2	$(t_{2g})^5$	1.28	0.28	1.17	24
	+1	4/2	$(t_{2g})^4(e_g)^2$	4.67	0.67	1.13	59
		0	$(t_{2g})^6$	0.72	0.72	1.93	37
Fe	+2	0	$(t_{2g})^6$	0.23	0.23	0.76	30
Co	+2	1/2	$(t_{2g})^6(e_g)^1$	1.08	0.08	0.51	16
	+1	2/2	$(t_{2g})^6(e_g)^2$	2.54	0.54	0.94	57
Ni	+2	2/2	$(t_{2g})^6(e_g)^2$	1.84	-	0.07	-
Cu	+2	1/2	$(t_{2g})^6(e_g)^3$	0.92	-	0.17	-
Zn	+2	0	$(t_{2g})^6(e_g)^4$	0.07	-	(0)	-
$BrMn(CO)_2L$	0		$(t_{2g})^6$	0.30	0.30[e]	0.67	<44[e]

[a] See ref 9. [b] Without a priori ligand reduction. [c] From Table 2; included here for comparison. [d] Biradical transfer as percentage of total transfer. [e] Includes transfer to CO ligands.

ZnL_2^{2+} complex (0.07 *e*).[18] These results should be treated with caution, since the basis set employed is not large enough for an accurate correlation treatment. Since we are primarily interested in wave function analysis, however, we feel that the results are still meaningful. We conclude that low-spin MnL_2^{+} is best viewed as an extensively delocalized system with an important biradical contribution. For all other systems, electron transfer is smaller, but the percentage of biradical character of this transfer is always significant.

It is important to note here that the biradical character we calculate is not due to one *particular* electron or orbital. All three electron pairs in the metal "t_{2g}" set are unpaired to some extent and so contribute to the total biradical transfer given in Table 3.

The *biradical character* of the transfer is primarily determined by the overlap between metal 3d and ligand π* orbitals. A smaller overlap causes a weaker interaction and hence more biradical character. This is illustrated most clearly by the pair LS-MnL_2^{2+}/HS-MnL_2^{+}, where—with a similar total transfer—the latter species has much larger M−N distances, leading to an increase in the biradical contribution from 24 to 59%. A similar increase (from 16 to 57%) is seen in the pair CoL_2^{2+}/CoL_2^{+}. Different factors control the magnitude of the transfer and its biradical contribution, and we find no clear correlation between magnitude of transfer and percentage of biradical character.

Conclusions

Despite the delicate balance between metal 3d and ligand π* orbitals, the B3LYP/SV level is sufficient to reproduce the main geometrical features of ML_2^{x+} complexes. The results obtained here support the conclusion[1] that in these complexes the ligand is non-innocent. In particular, the ECEC mechanism for the redox cycle of MnL_2^{2+} is confirmed. The analysis of the electronic structure of the complexes requires more elaborate calculations. In this particular case, where analysis of a correlated wave function based on Hartree−Fock orbitals was considered unreliable, a new CI approach based on (U)B3LYP orbitals appears to work satisfactorily. Analysis of the unpaired electron density, as proposed by Staroverov and Davidson,[9] indicates that MnL_2^{+} is best described as an extensively d → π* delocalized system with an important $Mn^{III}(d^4\text{-LS})(L^{-})_2$ biradical contribution.

(18) In test calculations on small molecules (alkanes, alkenes) we usually obtain UED's of around 0.02 for H and 0.05−0.10 for C. A value of ≈0.02−0.03 per electron pair appears to be "normal".

On the basis of the experimental data, a description of CoL_2^+ as a high-spin Co^{II} antiferromagnetically coupled to a ligand radical anion, was *not* considered likely.[1] Nevertheless, the large biradical contribution (0.54 *e*) indicates that this description significantly contributes to the electronic structure of CoL_2^+.

In the context of paired vs biradical electron transfer, diiminopyridine complexes appear to be borderline cases. With a somewhat smaller overlap between metal and ligand orbitals, the result would be a "pure" biradical in many cases (cf. the semiquinone complex mentioned earlier). With a somewhat larger overlap, one would obtain a regular back-donation situation. The fluidity of the bonding situation may be relevant to the usefulness of diiminopyridine complexes in catalytic applications.[19]

Acknowledgment. We thank the Dutch National Computing Facility (NCF) for generous amounts of computer time.

Supporting Information Available: Tables of bond lengths (S4) and deformations (S5) calculated at the B3LYP/sto-3g level; Mulliken analyses of electron transfer (S6); total energies (3-21G and sto-3g) for all species mentioned in the text (S7). This material is available free of charge via the Internet at http://pubs.acs.org.

IC001457C

(19) See, for example: Arana, C.; Yan, S.; Keshavarz-K, M.; Potts, K. T.; Abruña, H. D. *Inorg. Chem.* **1992**, *31*, 3680. Small, B. L.; Brookhart, M.; Bennett, A. M. A. *J. Am. Chem. Soc.* **1998**, *120*, 4049. Small, B. L.; Brookhart, M. *Macromolecules* **1999**, *32*, 2120. Britovsek, G. J. P.; Gibson, V. C.; Kimberley, B. S.; Maddox, P. J.; McTavish, S. J.; Solan, G. A.; White, A. J. P.; Williams, D. J. *Chem. Commun.* **1998**, 849. Britovsek, G. J. P.; Bruce, M.; Gibson, V. C.; Kimberley, B. S.; Maddox, P. J.; Mastroianni, S.; McTavish, S. J.; Redshaw, C.; Solan, G. A.; Stromberg, S.; White, A. J. P.; Williams, D. J. *J. Am. Chem. Soc.* **1999**, *121*, 8728. Britovsek, G. J. P.; Mastroianni, S.; Solan, G. A.; Baugh, S. P. D.; Redshaw, C.; Gibson, V. C.; White, A. J. P.; Williams, D. J.; Elsegood, M. R. J. *Chem. Eur. J.* **2000**, *6*, 2221. Reardon, D.; Conan, F.; Gambarotta, S.; Yap, G.; Wang, Q. Y. *J. Am. Chem. Soc.* **1999**, *121*, 9318.

(20) Meehan, P. R.; Alyea, E. C.; Ferguson, G. *Acta Crystallogr.* **1997**, *C53*, 888.